

Influence of the Local Urban Environment on the Thermoradiative and Hydrological Behavior of a Garden Lawn

AUDE LEMONSU,^a CÉCILE DE MUNCK,^a EMILIE REDON,^a VALÉRY MASSON,^a PASCAL KERAVEC,^b
FABRICE RODRIGUEZ,^c LAETITIA PINEAU,^c AND DOMINIQUE LEGAIN^d

^a CNRM, Université de Toulouse, Météo-France, CNRS, Toulouse, France

^b LHEEA, Centrale Nantes, CNRS, Nantes, France

^c GERS-LEE, Université Gustave Eiffel, IFSTTAR, F-44344 Bouguenais, France

^d Météo-France, Direction des Systèmes d'Observation/Département de l'Observation Territoriale, Saint Mandé, France

(Manuscript received 9 April 2021, in final form 7 September 2021)

ABSTRACT: Several urban canopy models now incorporate urban vegetation to represent local urban cooling related to natural soil and plant evapotranspiration. Nevertheless, little is known about the realism of simulating these processes and turbulent exchanges within the urban canopy. Here, the coupled modeling of thermal and hydrological exchanges was investigated for a lawn located in an urban environment and for which soil temperature and water content measurements were available. The ISBA diffusive (ISBA-DF) surface–vegetation–atmosphere transfer model is inline coupled to the Town Energy Balance urban canopy model to model mixed urban environments. For the present case study, ISBA-DF was applied to the lawn and first evaluated in its default configuration. Particular attention was then paid to the parameterization of turbulent exchanges above the lawn and to the description of soil characteristics. The results highlighted the importance of taking into account local roughness related to surrounding obstacles for computing the turbulent exchanges over the lawn and simulating realistic surface and soil temperatures. The soil nature and texture vertical heterogeneity are also key properties for simulating the soil water content evolution and water exchanges.


KEYWORDS: Energy budget/balance; Evapotranspiration; Soil moisture; Soil temperature; Land surface model; Urban meteorology

1. Introduction

Numerous recent studies based on numerical or experimental approaches are interested in the role of vegetation and pervious natural soils on local microclimate and thermal comfort in cities. Different physical and biophysical processes related to structural and functional characteristics of natural covers come into play. The radiative properties (albedo and emissivity) of natural covers can differ from those of artificial materials and hence modify the reflective properties of the environment (Santamouris 2013). For ground-based surfaces, for example, the albedo of bare soil or of grass is higher than that of asphalt streets, which significantly modulates the energy absorbed by the surface. The radiative exchanges in the urban canopy are also more deeply modified in the presence of trees: the foliage intercepts and absorbs part of the incoming radiation and hence reduces the direct radiation received by walls and ground-based surfaces (Souch 1993; Berry et al. 2013). Heat capacity and thermal conductivity also differ for natural soils in comparison with impervious covers properties (Oke et al. 2017) and evolve with time depending on soil water content dynamics. This changes the heat conduction flux in the ground. In addition, the water retention by natural soils, the resulting evaporation, along

with the plants' transpiration, injects water into the atmosphere while consuming a part of net energy of the system through the water phase change from liquid to vapor. Finally, the plant canopy, according to its nature (its composition, its height, its density of foliage) influences the local air flows and the intensity of turbulent exchanges (Banerjee et al. 2017; Kent et al. 2018). Therefore, the presence of pervious covers and vegetation in urban environments changes the partitioning of turbulent exchanges as sensible and latent heat, which is expressed by an often lower Bowen ratio (Christen and Vogt 2004) and higher evaporative fraction (Templeton et al. 2018). In conclusion, the radiation, energy, and water budgets of the whole urban canopy layer can be substantially modified by the presence of natural covers, and the local air temperature and humidity that result from these budgets are consequently influenced.

Inversely, the urban context in which these natural covers are constrained potentially disrupts the dynamical and biophysical processes usually observed in a purely natural environment. The proximity of impervious surfaces and of multiple built-up obstacles are expected to have an impact on the surface exchanges and the local microclimatic conditions to which urban vegetation is exposed. The functioning of plants could be additionally affected by the deeply disturbed and heterogeneous urban subsoil. However, few experimental campaigns document the fine-scale radiative, energetic, turbulent, or hydrologic interactions between local vegetation and urban infrastructures. This requires complex measurement protocols and instrumentation due to the fine scale of study and to the multiple processes that are involved. Some experimental studies proposed interesting methodological

 Denotes content that is immediately available upon publication as open access.

Corresponding author: Aude Lemonsu, aude.lemonsu@meteo.fr

DOI: 10.1175/JAMC-D-21-0067.1

© 2022 American Meteorological Society. For information regarding reuse of this content and general copyright information, consult the [AMS Copyright Policy \(www.ametsoc.org/PUBSReuseLicenses\)](#).

and technical approaches, with a more specific attention to the role of trees. [Pataki et al. \(2011\)](#) have extended the technique of sap-flux measurements to mature urban trees of various species to study their transpiration. [Shashua-Bar et al. \(2009\)](#) conducted an innovative experiment in setting up courtyards with different plant systems. The landscaping and the instrumentation were controlled with the objective to dissociate the irrigation of the lawn and the trees and to measure separately their evapotranspiration (by lysimeters and sap-flow systems, respectively). [Zhao et al. \(2018\)](#) quantified the cooling effect of tree shading using an urban physical-scale model with concrete blocks for buildings and artificial trees. Without taking into account the physiology of trees, this study nevertheless made it possible to experimentally treat their radiative effects for different layouts and densities. The investigation of local environmental factors that can influence evapotranspiration (ET) of urban lawns is addressed in some agronomic studies because, as stated by [Snyder et al. \(2015\)](#), urban irrigation raises water management and optimization issues similar to those found in agriculture. The study of irrigated turfgrass makes it possible to focus on microclimatic factors and their possible disruption by the urban environment, independently from any effect related to water resources and heat stress. Indeed, in contrast to grass fields, city lawns are small and close to urban landscape elements of various kinds ([Litvak et al. 2014](#)) that may especially change local radiation and wind conditions. Shading of trees (or obstruction by buildings) reduces the incoming radiation received by the lawn and the net energy absorbed, that plays a key role in limiting ET ([Shashua-Bar et al. 2009](#); [Litvak et al. 2014](#)). The proximity of trees can also offer a turbulent sheltering for ground-based vegetation creating a wind shadow effect that reduces the surface/atmosphere exchanges ([Green et al. 2021](#)). Conversely, ET of unshaded lawns can be enhanced by air advection coming from warmer impervious areas nearby ([Oke 1982](#)). In addition, the urban morphology tends to slow down the wind speed, which limits turbulent exchanges and may significantly reduce ET ([Snyder et al. 2015](#)).

Concomitantly, the numerical modeling has progressed in recent years toward a better representation of natural covers in urban climate models ([Lee and Park 2008](#); [Lee 2011](#); [Lemonsu et al. 2012](#); [de Munck et al. 2013](#); [Wang et al. 2013](#); [Krayenhoff et al. 2014, 2015, 2020](#); [Ryu et al. 2016](#); [Redon et al. 2017, 2020](#)). The implementation of such processes and of the interactions between vegetation and built-up infrastructures at a small scale is particularly crucial in numerical studies investigating urban design strategies for improving thermal comfort. This remains a critical point noted by [Krayenhoff et al. \(2021\)](#) in their review of works on urban cooling. For ground-based vegetation, a specific attention has been paid to the representation of radiative exchanges and the evaluation of parameterizations ([Krayenhoff et al. 2014](#); [Ryu et al. 2016](#); [Redon et al. 2017](#)), and to the drag effects of trees on the airflow within the canyon ([Krayenhoff et al. 2015](#); [Redon et al. 2020](#)). But very few studies evaluate and discuss the impacts of the surrounding urban landscape and soil water resource evolution on the modeling of soil evaporation and

plant transpiration. For very specific and short-term case studies, [Lemonsu et al. \(2012\)](#) present a good comparison between lawn evaporation measured in situ by a lysimeter and simulated by the Town Energy Balance (TEB) model including ground-based vegetation; [Wang et al. \(2013\)](#) show that their urban model, which integrates natural soil hydrology modeling, simulates realistic soil water content also for an urban lawn. In both examples, there is little discussion of soil and vegetation characteristics.

Among the urban canopy models cited, the ground-based surface in TEB model has been integrating a patch of vegetation within the canyon besides artificial materials since the works of [Lemonsu et al. \(2012\)](#) and [Redon et al. \(2017, 2020\)](#). The thermal and hydrological exchanges in the natural soil and at the interface with atmosphere, as well as the physiological functioning of vegetation, are simulated by the Interactions between Soil, Biosphere, and Atmosphere (ISBA) model with its diffusive (ISBA-DF) version ([Boone et al. 2000](#); [Decharme et al. 2011](#)). The vegetation can influence the air temperature and humidity conditions in the canyon through the energy fluxes it generates. The turbulent heat exchanges at the interface between the lawn and the ambient air are calculated by taking into account the temperature gradient, and an exchange coefficient that depends on the wind speed and the roughness of the lawn. The formulation for the turbulent water vapor exchanges is more complex because it involves different mechanisms: water evaporation from the ground, direct evaporation of water intercepted on leaves, and plant transpiration. Since the grassed surfaces are placed in the canyon, the radiation, water, and energy balances are calculated taking into account the geometry and layout of the canyon that constrains the amount of radiation received by the surface and exchanged with the other elements of the environment, as well as the microclimatic conditions of temperature, humidity, and wind near the surface. So far, while parameterizations have been progressively refined to better represent processes and process interactions, little effort has been made on input data. The characteristics of urban vegetation, both physiological and morphometric, were prescribed in previous studies with standard and default values ([Lee 2011](#); [Daniel et al. 2018](#); [de Munck et al. 2018](#)).

The objective of our study is to investigate more closely the coupled modeling of thermal and hydrological exchanges for a lawn located in an urban environment. This work is based on experimental data from the 1-month FluxSAP campaign ([Rodriguez et al. 2015](#)), which took place in the city of Nantes, France, and during which a specific instrumentation has been set up in a private garden. Meteorological variables (temperature, humidity, wind, and radiation) were measured near the surface so that they could incorporate the disturbances related to the urban elements close by. This experimental configuration enables to focus on the ability of surface-vegetation-atmosphere transfer models to simulate the thermal and hydrological behavior of the lawn. This is done using ISBA-DF, first evaluated in its default configuration. Then particular attention is paid to the parameterization of turbulent exchanges above the lawn, and to the description of soil characteristics. These issues are addressed using and adapting

ISBA-DF, with the aim to discuss potential needs for new urban data, and possible improvements to the parameterizations for future applications of TEB to vegetated urban canyons.

2. Presentation of experimental data

a. Study area and observation time period

A large experimental program called FluxSAP dedicated to the hydroclimatological monitoring of the urban environment was carried out in 2012 in the city of Nantes (Rodriguez et al. 2015) at the scale of a large neighborhood. The study area is located within the Observatory for Urban Environments of Nantes (ONEVU), devoted to the study of water, pollutant, and energy balances since 2006 (Ruban et al. 2007). Among the experimental sites, a specific instrumentation was set up in a private garden, with sensors installed over the lawn and in the ground in order to document the surface radiative and energy exchanges in parallel to the soil status evolution (temperature and moisture) on a more local scale. The study site is within an old working-class neighborhood of Nantes called Grand Clos, located 3.5 km northeast of Nantes city center. It was built after the Second World War to rehouse the disaster-stricken population. It has a very regular spatial organization and architecture (Fig. 1). Streets follow approximately north–south- and east–west-oriented axes. Houses are all identical, two-story (about 8 m high), semidetached, and organized in regular north–south bands. The back deck of the houses opens onto a long garden (about 12 m wide and 28 m long, i.e., an area of 340 m²) with a tree. Gardens are separated from each other by small hedges, and most of the houses have a garage or storeroom at the back of the garden.

The observation period ran from 0030 UTC 24 May 2012 to 2330 UTC 26 June 2012, corresponding to the spring season in France. The evolution of radiative and atmospheric conditions over time (Fig. 2) showed that the meteorological conditions changed during the experimental campaign. The first 10 days from 24 May to 2 June corresponded to a sunny period with maximum daily temperatures up to 29°C and high daily amplitudes from 10° to 15°C. Weather conditions subsequently changed from 3 to 14 June, with short but daily rainfall events (leading to a recharge of soil water reservoirs) and a shift to a westerly regime with a strengthening of the wind. A significant cooling was observed with maximum temperatures not exceeding 20°C and a strong decrease in daily temperature amplitude. At the end of the campaign, conditions were more variable. A few rainy passages persisted but temperatures rose again slightly.

b. Experimental design for the study of the lawn

The garden was equipped with different sensors (Fig. 3). Local meteorological parameters were monitored by a weather station installed over the lawn at 2 m above the ground for measuring air temperature and humidity, as well as a rain gauge. Two levels of wind measurement were carried out, that is, at 2 m with a cup anemometer (R.M. Young Co. 05106) and at 0.80 m with an ultrasonic anemometer (Gill HS-50). An infrared thermometer provided leaf surface

temperature measurements, and a temperature probe was installed on the lawn to measure the temperature of the surface soil layer. Three couples of probes for soil temperature and soil water content were installed at 0.10-, 0.35-, and 0.65-m depths to monitor the thermal and hydrological behaviors of the ground. Downward and upward shortwave (S^\downarrow and S^\uparrow) and longwave (L^\downarrow and L^\uparrow) radiation was also recorded by a radiometer installed at 0.80 m above the lawn. The net radiation Q^* (W m⁻²) was deduced according to

$$Q^* = S^\downarrow + L^\downarrow - (S^\uparrow + L^\uparrow). \quad (1)$$

In addition to the garden measurements, meteorological data of temperature and wind components (uSonic Metek USA-1 sonic anemometer), along with radiation and energy fluxes, were also recorded at the top of a 26-m-high mast, that is, above the top of the urban canopy layer and beyond the roughness sublayer. The mast was installed on an open sport field 400 m east of the site.

3. Analysis of in situ surface roughness conditions

a. Comparison of multilevel wind measurements

During the experiment, measurements of horizontal wind speeds were collected at three different vertical levels: at $z_{26m} = 26$ m above ground level a few hundred meters east of the garden (i.e., above the roughness sublayer) and at two levels inside the garden at $z_{2m} = 2$ m and $z_{0.8m} = 80$ cm. At 26 m high, wind speed varied on average between 2 and 7 m s⁻¹ with a marked diurnal cycle and higher wind speeds during daytime than nighttime (Fig. 4, top). The wind was strongly slowed down in the urban canopy layer. Measurements recorded in the garden highlighted comparable diurnal cycles but with much lower wind speeds, systematically below 2 m s⁻¹. In addition, the different measurement levels showed an effect of obstacles on the flow direction (Fig. 4, bottom). The regular arrangement of houses as parallel rows in the neighborhood can be seen as a combination of street-side and garden-side canyons, with respective aspect ratios of 0.25–0.30 for the street-side canyons and 0.10–0.13 for the much wider garden-side canyons (see aerial photograph in Fig. 1). According to the literature, the theoretical flow regime that develops in the roughness sublayer for that range of aspect ratios is the isolated roughness flow (Oke et al. 2017): obstacles are far enough from each other to form isolated wakes with very small interobstacle interactions. The comparison of wind directions between 26 (above buildings) and 2 (in the garden) m showed predominant wind sectors. The large-scale flow preferentially arrived from west-southwest to west-northwest (i.e., mainly from 225° to 315° in relation to the mean direction of building rows), whereas the flow in the garden was rather from southeast. A different change of direction was noted at a height of 80 cm. The flow was always from east (90°–135° in relation to the orientation of building rows). A precise interpretation of the flow regimes in the garden is difficult with only the available measurements. Nonetheless, the observed changes in direction could result from the effect of regular



FIG. 1. Aerial photograph of the study site (source of map data: Google Maps) with location of the instrumented garden and of the 26-m flux measurement mast, and street picture of the neighborhood (source: copyright S. Marc). The inset diagram in the upper photograph describes how the 45° wind sectors are defined according to the mean orientation of the rows of houses.

rows of buildings to which is locally added the effect of the small obstacles (e.g., hedges, garages, storerooms) located in the gardens.

b. Evaluation of aerodynamic roughness length

We explored the possibility of evaluating the roughness characteristics of the site at two spatial scales, that is, for

the whole urban canopy layer, and in the garden within the urban canopy layer. During the FluxSAP experiment, only one level of wind speed measurement above the top of the buildings (at 26 m above ground level) was available, which did not allow one to estimate the associated displacement height z_d and aerodynamic roughness length z_{0m} using the classical micrometeorological (or anemometric) method.

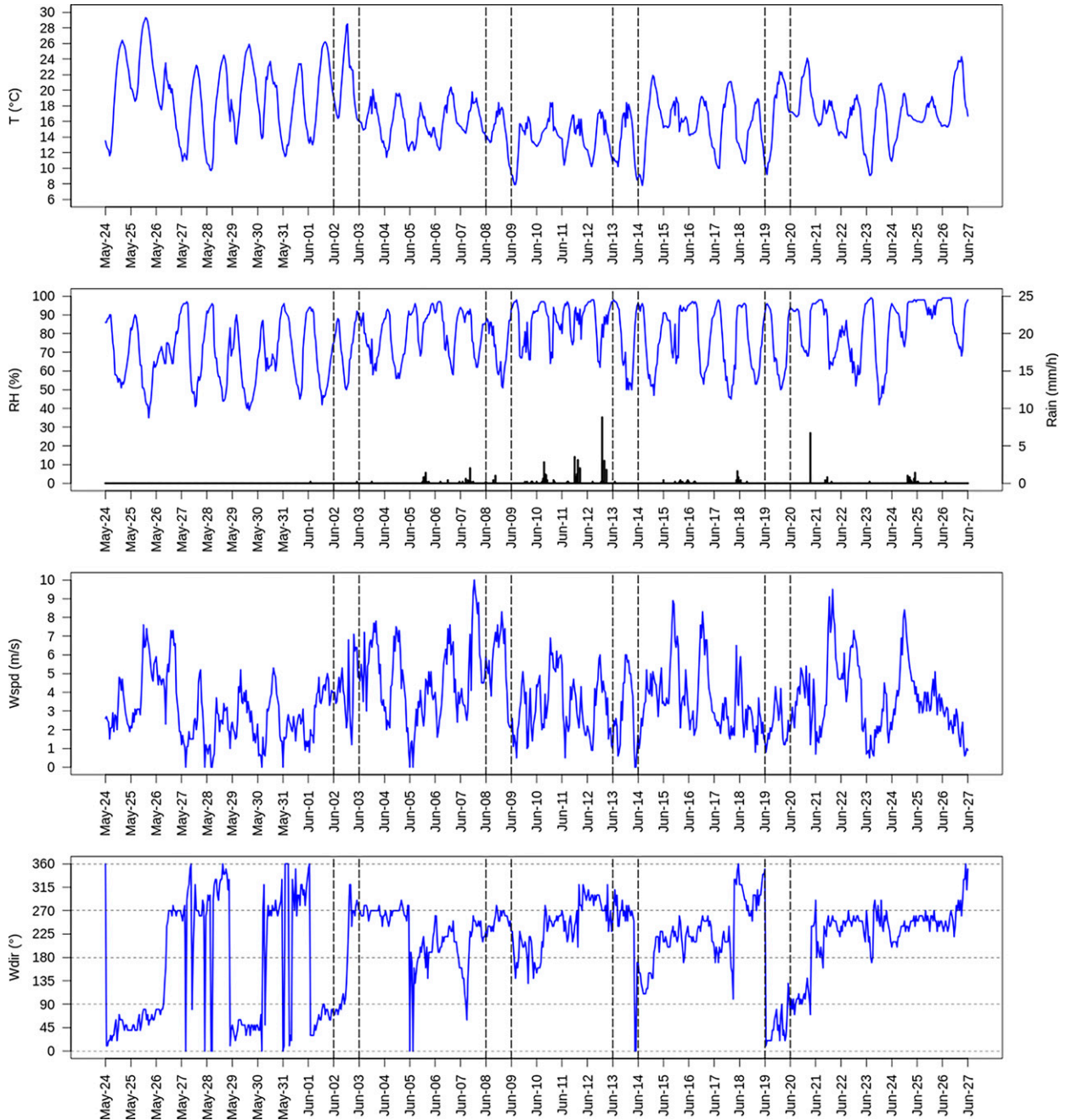


FIG. 2. Synoptic meteorological conditions [(top) air temperature, (top middle) relative humidity and rain rate, (bottom middle) wind speed, and (bottom) wind direction] recorded at Nantes airport operational weather station during the FluxSAP field experiment. The vertical dashed lines indicate the dates selected for the analysis of the temperature and humidity vertical profiles (section 5).

These estimates could be carried out during the preparatory campaign that took place in 2010, during which the mast was instrumented on three levels of altitude (16, 21, and 26 m) with a cup anemometer at the lowest level and two sonic anemometers above. Bagga (2012) computed z_d and z_{0m} by wind sectors, using multilevel data of horizontal wind speed $u(z)$ and the averaged friction velocity u_* , and according to the logarithmic wind profile formulation based

on Monin–Obukhov similarity theory in neutral condition (κ is the von Kármán constant):

$$u(z) = \frac{u_*}{\kappa} \ln\left(\frac{z - z_d}{z_{0m}}\right). \tag{2}$$

For the urban canopy layer and depending on wind sector, it was found that z_d varied between 5.5 and 10 m with a mean value of about 8 m and that z_{0m} varied between 0.5 and 1.5 m.

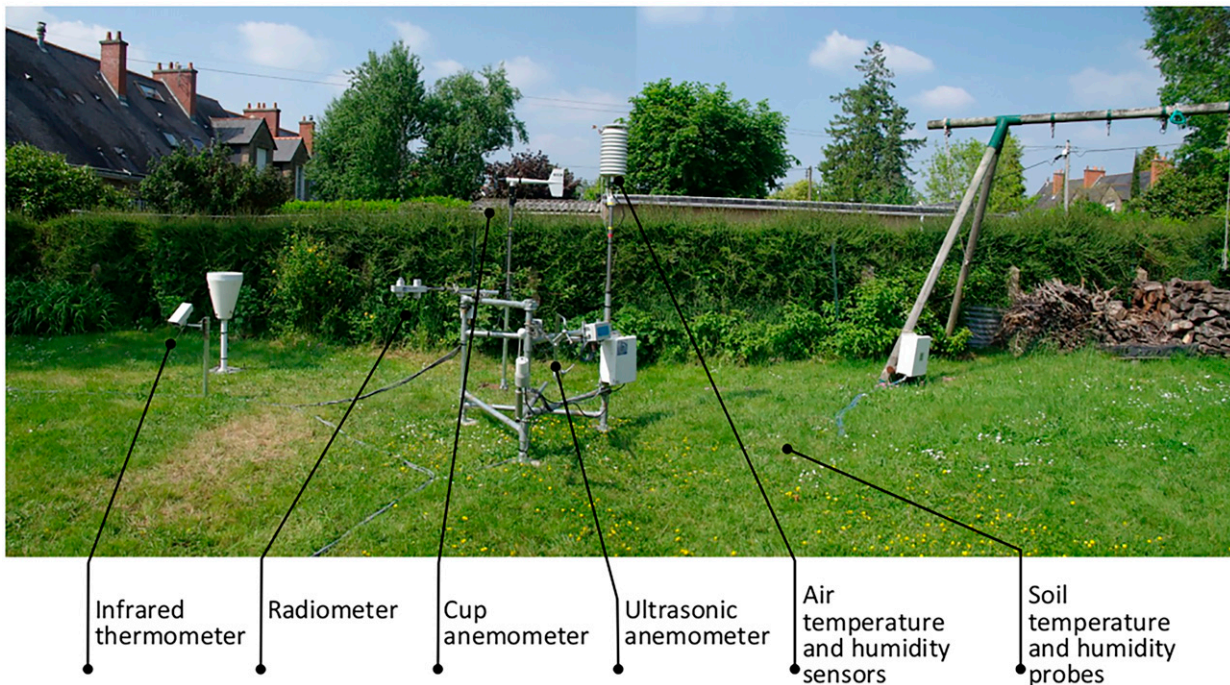


FIG. 3. Description of the instrumentation implemented in the private garden.

We then estimated the order of magnitude of the aerodynamic roughness length relative to the turbulent exchanges over the lawn (i.e., inside the urban canopy layer) on the basis of a simple morphometric approach. The height and surface area of the main obstacles present in the garden were defined using cadastral data and aerial photograph of the site. The hedge and the fence bordering the garden were about 1.20 m high for a total area of 18 m². The height of the garage was 2 m and its surface area was 43 m². The tree in the middle of the garden was about 6 m high, and its crown was 5 m in diameter. A drag coefficient was calculated independently for each element by assuming a roughness length equal to 1/10 of the element height and a reference height z_{ref} of 2 m, according to

$$C_D = \left[\kappa / \ln(z_{\text{ref}}/z_{0m}) \right]^2. \quad (3)$$

An average drag coefficient was derived by weighting the drag coefficients according to the surface areas associated with each element. The average aerodynamic roughness length was then calculated by inverting Eq. (3) giving a value of 0.32 m.

4. Presentation of ISBA model and numerical experiment

The ISBA model is a soil–vegetation–transfer model that allows the representation of natural soils and vegetation in meteorological, climatic, or hydrological models. It models water and heat transfers in the soil, surface hydrology, and the evapotranspiration functioning of vegetation. Since the

ISBA standard force–restore version (Noilhan and Planton 1989), various advances have been made and different configurations exist today. The first coupling studies between ISBA and TEB for the representation of urban vegetation (Lemonsu et al. 2012) were based on ISBA 3-L (Boone et al. 1999), which describes the soil column with three layers (surface, root, and deep layers). Now it is the multilayer version of ISBA, also called diffusive and noted ISBA-DF (Boone et al. 2000; Decharme et al. 2011) that is preferred, because it allows the soil to be discretized more realistically into a greater number of layers and to explicitly address the vertical water transfers that result from soil moisture gradients. For the calculation of energy exchanges, the model is based on the big-leaf approach, which is a simplification in the representation of natural cover. They are treated as a homogeneous composite canopy including soil and vegetation for which a single surface energy balance is calculated and a single equation for temperature evolution is solved. The surface exchanges with the atmosphere are calculated based on the Monin–Obukhov similarity theory (MOST; Monin and Obukhov 1954) by assuming horizontal homogeneity conditions and characteristic displacement height and roughness length for the canopy.

a. Definition of atmospheric conditions

The ISBA-DF model was applied to a single grid point, centered on geographic coordinates of the study area 47°14'38"N, 1°31'56"W, since the objective was here to study very local processes at the scale of the lawn by assuming that there was no large-scale effect. The model was run in offline mode, that is, without explicit coupling with an atmospheric model but forced using local observations. The atmospheric

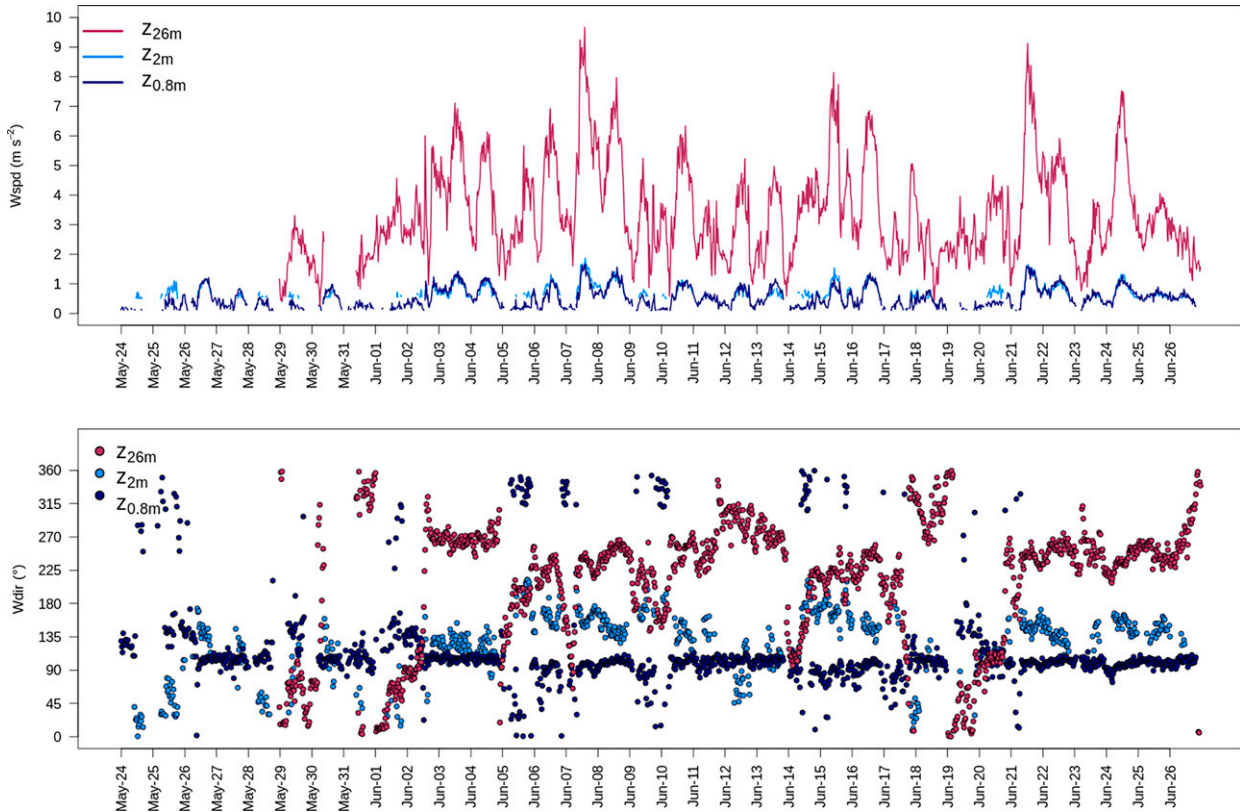


FIG. 4. Time series of (top) wind speed and (bottom) wind direction recorded at the top of the mast (26 m above the ground) and at 2-m and 80-cm height in the garden.

conditions were defined from 24 May to 26 June 2012 with a uniform time step of 30 min. In accordance with the instrumentation setup, air temperature, humidity, and pressure, as well as wind speed, were applied at an altitude of 2 m above the ground. The radiative forcing conditions were deduced from radiation measurements that included incoming global shortwave radiation and incoming longwave radiation. The incoming global solar radiation S_g was partitioned into direct (S^\downarrow) and diffuse (S^\uparrow) solar radiation contributions using the formulation of Erbs et al. (1982) that enables to compute the diffuse radiation fraction from a theoretical global radiation and the zenith angle.

b. Model configurations

The ISBA-DF model requires the prescription of an ensemble of input parameters relative to soil and vegetation (the main ones are listed in Table 1). For soil, it is necessary to define the soil texture (as a combination of sand, clay, and silt fractions), from which the thermal and hydrological properties are derived (all listed in Table 1). For vegetation, its type, density (characterized by the vegetation fraction, that is, the projected percentage of the ground that is vegetated (leaves) and the leaf area index), root profile in the ground (defined as root cumulative fractions in soil layers), reflective properties (albedo and emissivity), and roughness must be specified. In urban areas, when ISBA-DF is coupled to TEB for addressing

the local-scale interactions between built-up surfaces and vegetation (Lemonsu et al. 2012), these parameters are often quite difficult to define because of the heterogeneity and complexity of the environment, and because of the lack of information. The input parameters are therefore usually prescribed on the basis of default values or information from global databases, without any specific calibration. The uncertainties and errors associated with the definition of these parameters can have a significant impact on the results of the ISBA-DF model run at small scale, and ultimately on the urban microclimate simulated. These issues will be investigated in the next section.

1) VEGETATION PROPERTIES

Any ISBA-DF configuration combines two main datasets, one for vegetation characterization, and one for soil characterization (next subsection). The area of the garden that was instrumented during FluxSAP and is simulated with ISBA-DF was composed of grassy lawn. The grass remained green and healthy during the field campaign (see the photograph in Fig. 3), so that the vegetation fraction was prescribed to 100% and the leaf area index (LAI) to $2 \text{ m}^2 \text{ m}^{-2}$. A parameter defining the root exploration fraction by soil layers was also required. This governs the capacity of plants to extract available soil water for transpiration depending on root distribution and water content profiles. It is expressed as a vertical profile of root density (in cumulative percentage) that does

TABLE 1. Input parameters of the ISBA-DF model for the description of vegetation and soil properties in the different experiments (DEF, EXP1, EXP2, and EXP3).

	DEF	EXP1	EXP2	EXP3
Option for roughness	Z0M-GRASS	Z0M-GARDEN	Z0M-URBAN	Z0M-GARDEN
Option for soil texture	TXT-HWSD	TXT-HWSD	TXT-HWSD	TXT-INSITU
Type of vegetation	Grass	Vegetation parameters	Grass	Grass
Vegetation fraction (%)	100	Grass	100	100
Leaf area index ($\text{m}^2 \text{m}^{-2}$)	2	2	2	2
Vegetation emissivity	0.98	0.98	0.98	0.98
Vegetation albedo	0.20	0.20	0.20	0.20
Aerodynamic roughness length (m)	0.004	0.32	1.50	0.32
Depth of soil layers (cm)		<i>Soil description</i>		
Root cumulative fraction per layer (%)		1, 3, 5, 8, 12, 20, 30, 40, 50, 80, and 180		
Reference depths for soil texture definition (cm)		10, 20, 30, 50, 80, 100, 100, 100, 100, and 100		
Sand fraction (%)	0-180	0-180	0-180	20-50
Clay fraction (%)	37	37	37	50
Silt fraction (%)	24	24	24	14
	39	39	39	36
				30
				30
				40
Hydrological conductivity at saturation (m^{-1})	4.55×10^{-6}	<i>Hydrological properties</i>	4.55×10^{-6}	14.5×10^{-6}
Matrix potential at saturation (m)	-0.334	4.55×10^{-6}	-0.334	-0.270
<i>b</i> coefficient	6.789	-0.334	6.789	5.419
Water content at wilting point ($\text{m}^3 \text{m}^{-3}$)	0.182	6.789	0.182	6.652
Water content at field capacity ($\text{m}^3 \text{m}^{-3}$)	0.337	0.182	0.337	0.178
Porosity ($\text{m}^3 \text{m}^{-3}$)	0.454	0.337	0.454	0.280
Initial conditions for SWI at 10 cm	0.697	0.454	0.697	0.429
Initial conditions for SWI at 35 cm	0.510	0.697	0.510	1.099
Initial conditions for SWI at 65 cm	0.864	0.510	0.864	-
		0.864		0.787
		<i>Thermal properties</i>		-
Thermal conductivity of dry soil ($\text{W m}^{-1} \text{K}^{-1}$)	0.202	0.202	0.202	0.212
Thermal conductivity of soil matrix ($\text{W m}^{-1} \text{K}^{-1}$)	3.381	3.381	3.381	3.994
Heat capacity of dry soil ($\text{MJ m}^{-3} \text{K}^{-1}$)	1.979	1.979	1.979	1.979
				1.979
				2.69 $\times 10^{-6}$
				-0.385
				7.611
				0.203
				0.359
				0.462
				-
				-
				0.724
				0.197
				3.091
				1.979

not exceed here 20 cm to respect a realistic root depth for grass. In the absence of measurements, the thermal emissivity was set at 98% depending on the type of vegetation and on the basis of the emissivity values found in the literature for this type of vegetation, notably from satellite measurements (Qin and Karnieli 1999). The shortwave radiation measurements above the lawn made it possible to estimate the lawn albedo (not shown): based on the ratio between upwelling and downwelling radiation during daytime hours, the albedo was estimated to 20%. This value remained mostly stable for the first weeks of the field campaign, and a slight decline was observed after 10 June, which could be explained by a lawn cutting that occurred at that time.

Several options were tested for the surface roughness definition given the heterogeneity of the site. The homogeneous configuration of the lawn is consistent with the big-leaf simplification of ISBA and the MOST at the scale of the vegetation canopy. Nonetheless, since the lawn is located in the urban canopy layer, the validity of the MOST assumptions can be questioned. This point was already suggested by the analysis of the in situ data (section 3) that showed that aerodynamic roughness of the lawn could be influenced by the surrounding elements of the landscape, and not be only dependent on the lawn itself. As a consequence, z_{0m} was first prescribed according to the standard approach applied by ISBA-DF (and other surface-vegetation-atmosphere transfer model models) as equal to the tenth of the mean height of grass blades that are around 4 cm in height (option Z0M-GRASS = 0.004 m). For a purpose of comparison and sensitivity analysis, it was also prescribed two other ways: 1) by defining an aerodynamic roughness length of 0.32 m for the lawn, that is, the value obtained by the morphometric approach (option Z0M-GARDEN = 0.32 m); and 2) by testing the maximum value of 1.5 m corresponding to the roughness of the urban canopy estimated experimentally by Bagga (2012) (option Z0M-URBAN = 1.5 m).

2) SOIL CHARACTERISTICS

For ISBA-DF, the soil column is defined by a total depth and a vertical discretization according to a number of soil layers and associated thicknesses that are defined by the user. The soil discretization chosen here consisted in 11 layers whose thicknesses were fixed consistently with the depths of observed data in order to facilitate the comparison between observations and model estimates. The model needs as input the thermal properties of dry soil (heat capacity and thermal conductivity) and the hydrological properties of the soil (hydraulic conductivity at saturation, matrix potential at saturation, coefficient for water retention curve, water content at wilting point and field capacity, porosity). These properties are classically derived from the soil texture information, using the empirical pedotransfer formulations described in Boone et al. (2000) and Decharme et al. (2011). Without specific local data, which could allow a more realistic description of the complexity and heterogeneity of urban soils, the model usually operates with the Harmonized World Soil Database (HWSD; FAO/IIASA/ISRIC/ISSCAS/JRC 2012), which has

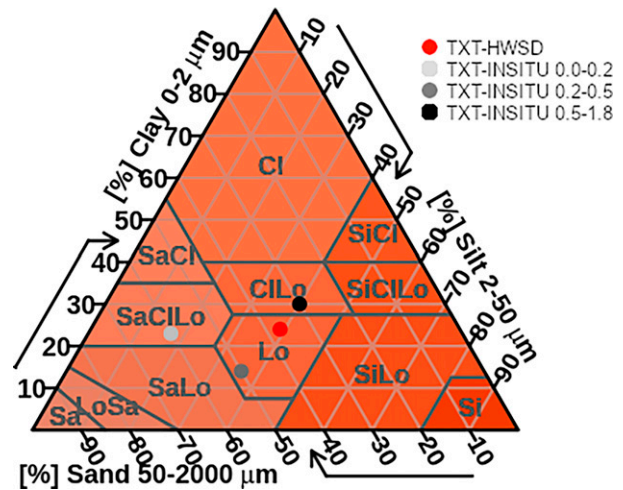


FIG. 5. Comparison of soil textures between options TXT-HWSD and TXT-INSITU (for the three soil depths) following the standard U.S. Department of Agriculture soil taxonomy. On the texture triangle, the labels “Sa,” “Cl,” and “Lo” refer to as sand, clay, and loam, respectively.

the advantage of being available everywhere on a continuous basis with a resolution of 30 arc s. For the studied area, according to these data, the soil is composed of 37% sand, 24% clay, and 39% silt. For clarity, this soil texture option is here called TXT-HWSD. It is plotted in Fig. 5 according to the standard soil taxonomy. Nevertheless, in a second step, the relevance of these soil texture data will be questioned and the sensitivity of the results to a more precise soil characterization will be investigated (section 5).

In summary, three experiments were first conducted and compared (section 5). The default experiment is referred to as DEF and combined the standard options Z0M-GRASS and TXT-HWSD as described before. The experiments EXP1 and EXP2 both applied the same soil texture option TXT-HWSD but with different roughness options Z0M-GARDEN and Z0M-URBAN, respectively. All properties for vegetation and soil, including thermal and hydrological properties derived from texture with the pedotransfer functions, are compiled in Table 1 for the different experiments conducted with ISBA-DF.

3) INITIAL CONDITIONS FOR SOIL STATUS

Soil moisture and soil temperature were initialized in accordance with observed data available at the various depths of 0.10, 0.35, and 0.65 m. Note that for the soil water status, the soil water contents were initialized in ISBA-DF through the soil wetness index (SWI):

$$\text{SWI} = \frac{w - w_{\text{wilt}}}{w_{\text{fc}} - w_{\text{wilt}}}. \quad (4)$$

This index expresses the soil moisture condition (as a fraction) by accounting for soil hydrological properties. It links together the difference between soil water content (w ; $\text{m}^3 \text{m}^{-3}$) and soil water content at wilting point (w_{wilt} ; same

TABLE 2. Statistical scores for soil water contents [RMSE ($\text{m}^3 \text{m}^{-3}$) and pBias (%)] and for soil temperatures [RMSE and mBias ($^{\circ}\text{C}$)] calculated for all sensitivity experiments between ISBA-DF results and in situ observations.

	DEF		EXPI		EXP2		EXP3	
	RMSE	pBias	RMSE	pBias	RMSE	pBias	RMSE	pBias
Soil water contents								
$w(10 \text{ cm})$	0.022	+6.20	0.022	+5.00	0.029	+7.74	0.021	-5.30
$w(35 \text{ cm})$	0.043	+16.47	0.041	+15.86	0.045	+17.25	0.019	-4.61
$w(65 \text{ cm})$	0.020	-6.01	0.020	-6.27	0.019	+5.64	0.008	+1.32
Soil temperatures		mBias		mBias		mBias		mBias
$T(\text{Surf})$	5.97	+2.21	3.11	-0.94	2.40	-1.57	2.96	-0.90
$T(\text{Lawn})$	4.93	+3.90	1.32	+0.75	1.90	+0.12	1.41	+0.80
$T(10 \text{ cm})$	3.74	+2.32	1.92	-0.60	1.78	-1.18	2.06	-0.50
$T(35 \text{ cm})$	2.57	+2.47	0.49	+0.10	0.61	-0.37	0.66	+0.24
$T(65 \text{ cm})$	2.18	+2.07	0.29	+0.23	0.24	-0.14	0.41	+0.34

units), and the difference between soil water content at field capacity (w_{fc} ; same units) and at wilting point. The SWI initialization was consequently defined according to the soil texture prescribed (hence the model-derived hydrological properties) and the initial water content at the three depths. The initial values of SWI for the different ISBA-DF configurations are listed in Table 1.

5. Evaluation of the modeling of heat and water transfers in the soil

The performances of ISBA-DF simulations were evaluated for the 30-min-time-step modeling of soil temperatures and water contents on the basis of three statistical scores, the root-mean-square error (RMSE, depending on the variable units), the mean bias (mBias, depending on the variable units), and the percent bias (pBias; %):

$$\text{RMSE} = \sqrt{\frac{\sum_{t=1}^n [x_{\text{OBS}}(t) - x_{\text{MOD}}(t)]^2}{n}}, \quad (5)$$

$$\text{mBias} = \frac{\sum_{t=1}^n [x_{\text{OBS}}(t) - x_{\text{MOD}}(t)]}{n}, \quad \text{and} \quad (6)$$

$$\text{pBias} = 100 \times \frac{\sum_{t=1}^n [x_{\text{OBS}}(t) - x_{\text{MOD}}(t)]}{\sum_{t=1}^n x_{\text{OBS}}(t)}, \quad (7)$$

with x_{MOD} being the modeled variable and x_{OBS} being the observed variable. The ensemble of statistical scores is gathered in Table 2 for soil temperature and soil moisture scores.

a. Evaluation of soil water contents

The first two weeks of field experiment were characterized by a dry period without important rainfall, so that a progressive drying of the soil has been observed (with a continuous decrease

in water content at 10-cm depth from 0.290 to 0.183 $\text{m}^3 \text{m}^{-3}$; Fig. 6). The following weeks, the water content increased again up to a maximum of 0.294 $\text{m}^3 \text{m}^{-3}$ due to successive rainfall events between the 5 and 13 June. Thereafter, soil moisture fluctuated between 0.250 and 0.270 $\text{m}^3 \text{m}^{-3}$ because of more sporadic rainfalls. The soil water contents recorded in the deeper layers (35- and 65-cm depths) indicated a slight but constant decrease of soil moisture all along the experimental period. At these depths and during this vegetation development season, the soil water status was clearly not sensitive to water input by precipitation at the surface.

The simulated water contents are compared at the 30-min time step with the in situ observations for the three measurement depths. It is noted that the simulated water content at 10-cm depth follows a diurnal cycle in response to the biophysical functioning of the vegetation, which is much less visible in the in situ measurements (Fig. 6, top panel). With the default configuration DEF, the model simulates relatively well the temporal variations in soil moisture near the surface with a RMSE of 0.022 $\text{m}^3 \text{m}^{-3}$ and a percent bias of 6.2% at 10-cm depth for the whole period (Fig. 6 and Table 2). At this level, the evolution of soil moisture is strongly correlated with the dynamics of lawn transpiration and the ability of the root system to extract water from the soil. The daily variations in the evaporative fraction, calculated from model outputs as the ratio of the turbulent latent heat flux to the sum of the turbulent fluxes $\text{EF} = Q_E / (Q_E + Q_H)$ (%) and presented in Fig. 7, show different transpiration regimes over the period. In the DEF experiment, EF is quite stable until 2 June (above 75%), indicating that the vegetation continues to transpire on a regular basis although there is no precipitation over the period. As a result, the soil gradually dries out to the depth to which the root system of the lawn extends, and the water content decreases down to 0.199 $\text{m}^3 \text{m}^{-3}$ in agreement with measurements. After 2 June, EF decreases down to 60% over a couple of days, then increases again from 5 to 14 June driven by new rainfall events, to remain stable until 23 June. These modulations in the transpiration regime explain in particular that the soil water content can increase again from 5 June, since the water losses by transpiration decrease. However, this reduction in transpiration seems to be overestimated by ISBA-DF when related to the observed water content: after

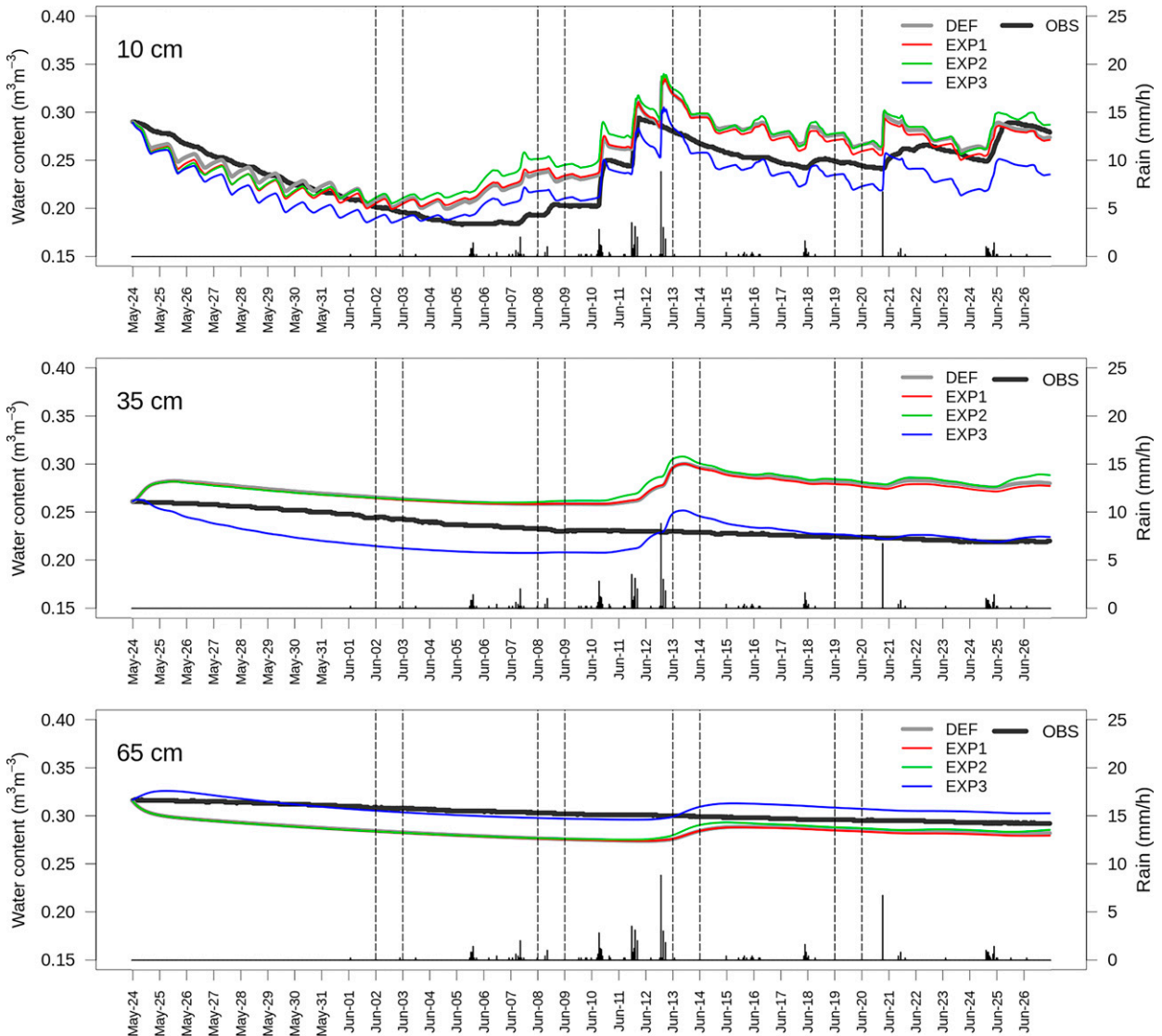


FIG. 6. Comparison of soil water contents simulated by ISBA-DF according to different configurations with in situ measurements at different depths in the soil column [(top) 10, (middle) 35, and (bottom) 65 cm]. The vertical dashed lines indicate the dates selected for the analysis of the temperature and humidity vertical profiles (section 5).

a first soil drying phase is well simulated, the soil water recharge with rainfall is a bit too fast and too important leading to a systematic overestimation of soil water content after the 5 June.

In general, the increase in roughness favors turbulent exchanges at the surface. If soil water availability is limited, these exchanges are preferentially in the form of sensible rather than latent heat flux. Consequently, the evaporative fractions of EXP1 (Z0M-GARDEN) and EXP2 (Z0M-URBAN), which display higher roughness lengths as DEF, are lower than that of DEF, as observed over the first part of the period until 11 June. EF decreases more clearly between 2 and 11 June in EXP2 (and to a lesser extent in EXP1), which explains why the soil water content in EXP2 is higher than in DEF during this period. After 11 June, the soil is recharged with water, so that the evaporative

capacity increases again for EXP1 and EXP2. As a result, the sensitivity of the evolution of water contents to surface roughness options becomes less visible at the end of the period.

At 35-cm depth, the modeled soil moisture is diverging with time and tends to overestimate the soil water content leading to a percent bias of +16%. Inversely, the simulated water content is underestimated by -6% in the deepest layer. Contrary to observations, it can be seen that the simulated water contents at 35- and 65-cm depth both increase around 12–13 June due to water vertical transfers from the more superficial soil layers. This finding possibly points a misprescription of soil texture and hydrological properties, that is discussed later. At these depths, the surface roughness options have little effect on the soil water content and scores are comparable.

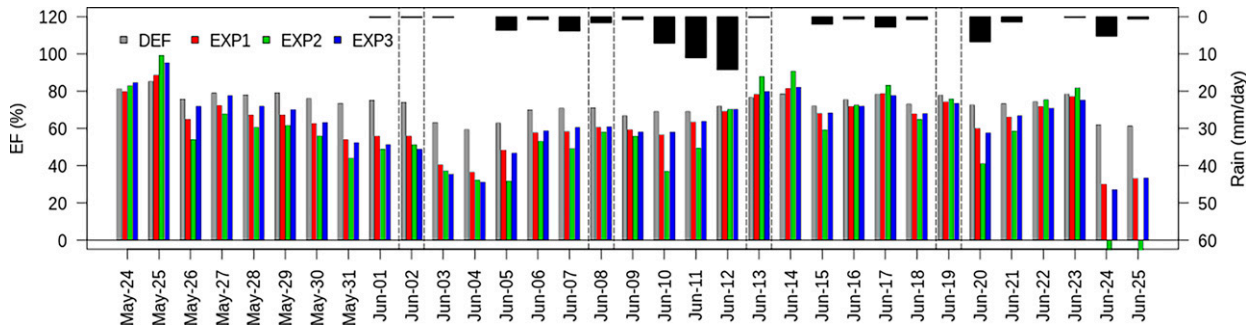


FIG. 7. Comparison of daily daytime evaporation fraction (expressed in percent) simulated by ISBA-DF for the different experiments. The thin vertical color bars represent the different experiments, and the downward black bars are the daily rainfall.

b. Evaluation of soil temperatures

With the big-leaf approach applied in ISBA (section 4), the first-level ground temperature T_{g1} is the temperature of a composite layer composed of the soil top layer and of grass. For evaluation purposes, this temperature was here compared with both the temperatures measured in the soil top layer $T(\text{Surf})$ and the surface temperature of the lawn $T(\text{Lawn})$ measured by an infrared thermometer (see instrumentation in Fig. 3). Observations indicate that the lawn surface temperature has a more important daily amplitude than soil top temperature, since it is driven by the surface radiation budget (Fig. 8). $T(\text{Lawn})$ is marked by a strong nocturnal cooling down to 5.4°C at minimum and daytime temperatures up to more than 34°C , while $T(\text{Surf})$ varies between 13.6° and 30.6°C with a mean temperature around 19°C . Below the surface, the soil temperature gradually decreases with depth. The diurnal cycle is significantly attenuated at 10-cm depth, then disappears at 35- and 65-cm depths. In comparison, the model in its default configuration DEF largely overestimates daytime temperature peaks whereas the simulated nocturnal temperatures are in the range of observed temperatures, and especially in good agreement with lawn surface temperature measurements (Fig. 8 and Table 2). The RMSE remains very high, that is, 6.0° and 4.9°C when comparing with $T(\text{Surf})$ and $T(\text{Lawn})$, respectively. The statistical scores are improved between the first and the deepest level with RMSE of 3.7° , 2.6° , and 2.2°C at 10-, 35-, and 65-cm depths, respectively, mainly due to the strong decrease in temperature daily amplitude. However, the model systematically overestimates the mean daily soil temperature in the entire soil column.

The comparison of experiments DEF, EXP1, and EXP2 conducted with ISBA-DF shows that the increase in roughness ($Z0M\text{-GRASS} < Z0M\text{-GARDEN} < Z0M\text{-URBAN}$) promotes turbulent exchanges between the surface and the atmosphere, which limits the surface warming at daytime much efficiently for EXP1 ($Z0M\text{-GARDEN}$) and EXP2 ($Z0M\text{-URBAN}$) than for DEF ($Z0M\text{-GRASS}$) (Fig. 8 and Table 2). A cooling is also noted at night relative to DEF but is far less important than during the day. The EXP2 ($Z0M\text{-URBAN}$) experiment is the configuration that gives rise to the strongest surface exchanges and therefore decreases the

most the diurnal temperature amplitude at and near the surface (at 10-cm depth). The difference between configurations is accentuated with the conditions of strong incoming radiation, warm surface temperatures, and lack of precipitation observed at the beginning of the period. In these conditions, the most realistic temperatures are simulated with the garden-scale aerodynamic roughness of 0.32 m (EXP1): for the surface, the RMSE is improved on average by more than 3°C and the mean bias is almost zero instead of $+3.0^{\circ}\text{C}$ for DEF. In comparison, the high roughness applied in EXP2 leads to too much cooling and a negative average bias of -0.7°C . Better performances are also noted in EXP1 for the other ground layers for which the overestimation in temperature is systematically reduced relative to DEF. The RMSE are only 1.9° , 0.5° , and 0.3°C at 10-, 35-, and 65-m depths, respectively, and mean biases are always lower than $\pm 0.6^{\circ}\text{C}$. Nevertheless, at 10-cm depth, even if the scores are globally better for EXP1 than for DEF, the cold nocturnal bias already noted in the DEF case is accentuated by $1^{\circ}\text{--}2^{\circ}\text{C}$ in EXP1.

To complete the analysis, vertical soil temperature profiles were calculated for daytime and nighttime by averaging the time frames 1300–1600 and 0100–0400 UTC, respectively (Fig. 9). The temporal dynamics of the temperature profiles observed during the study period in the soil column are well reproduced by the model. A gradual cooling takes place (both at daytime and nighttime) until 13 June then the soil warms up again at the end of the period. Both EXP1 and EXP2 significantly improve the temperature profiles relative to DEF, which simulates too warm soil temperatures over the whole soil column. At daytime, this improvement provided by the increase in surface roughness is noted for all measurement levels. The influence is more significant at the upper levels since the temperature profile dynamics is then driven by the radiation and energy turbulent surface exchanges. The comparison of EXP1 and EXP2 profiles confirms a slightly too strong cooling at the surface with EXP2 due to the very high surface roughness ($Z0M\text{-URBAN} = 1.5\text{ m}$). For deeper measurement levels, the two configurations give very similar results. At night, whereas energy exchanges between the surface and the atmosphere are reduced, the surface layers cool down by upward infrared emission. As mentioned previously, the nighttime cooling is a little too pronounced in the 0–20-cm

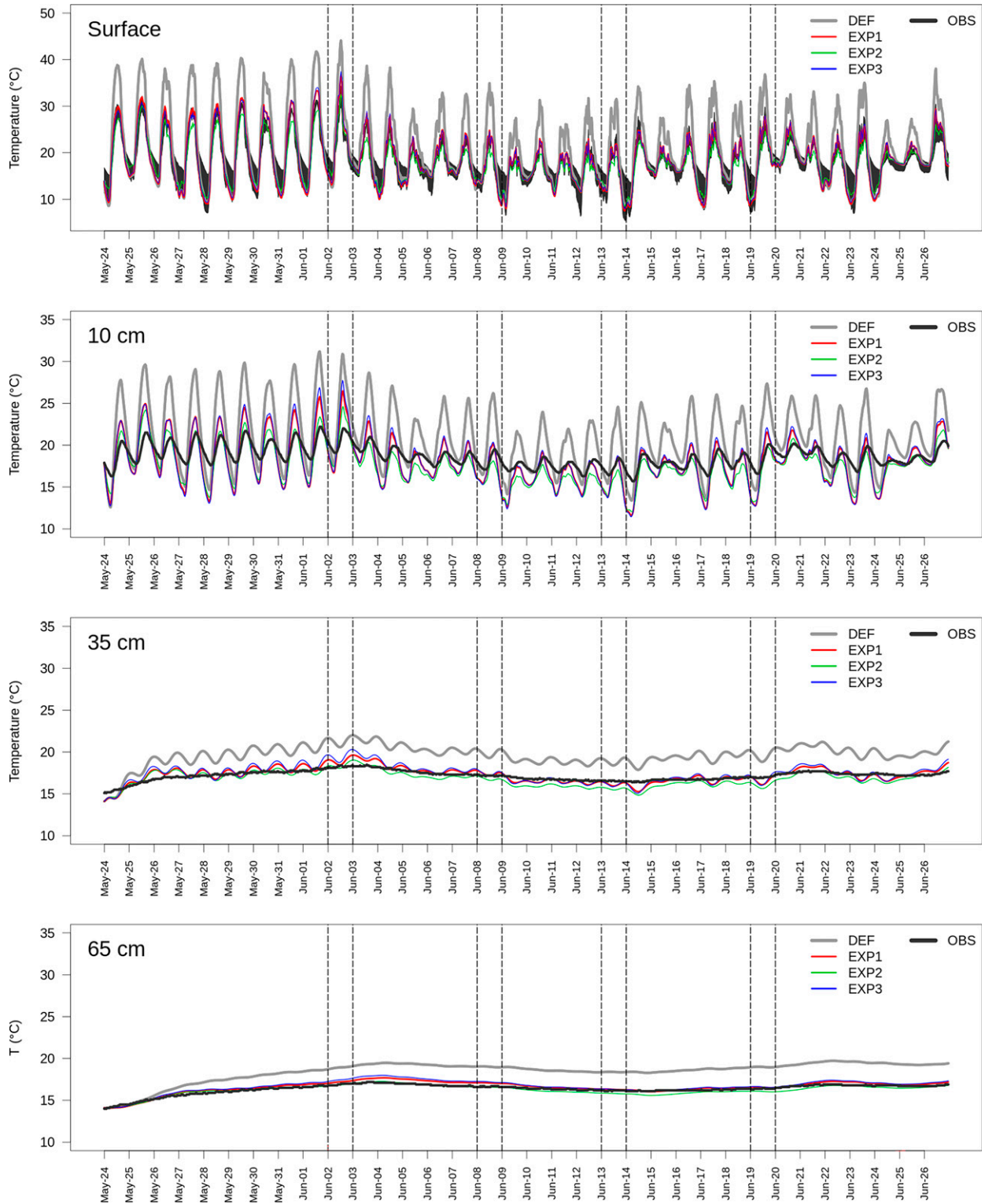


FIG. 8. Comparison of soil temperatures simulated by ISBA-DF according to the different configurations with in situ measurements at different depths in the soil column [(top) surface, (top middle) 10, (bottom middle) 35, and (bottom) 65 cm]. For the first level of ground, the observations, which combine measurements of near-surface soil temperature and lawn surface temperature, are presented as a black envelope to show the range of variation. The vertical dashed lines indicate the dates selected for the analysis of the temperature and humidity vertical profiles (Figs. 9 and 10, below).

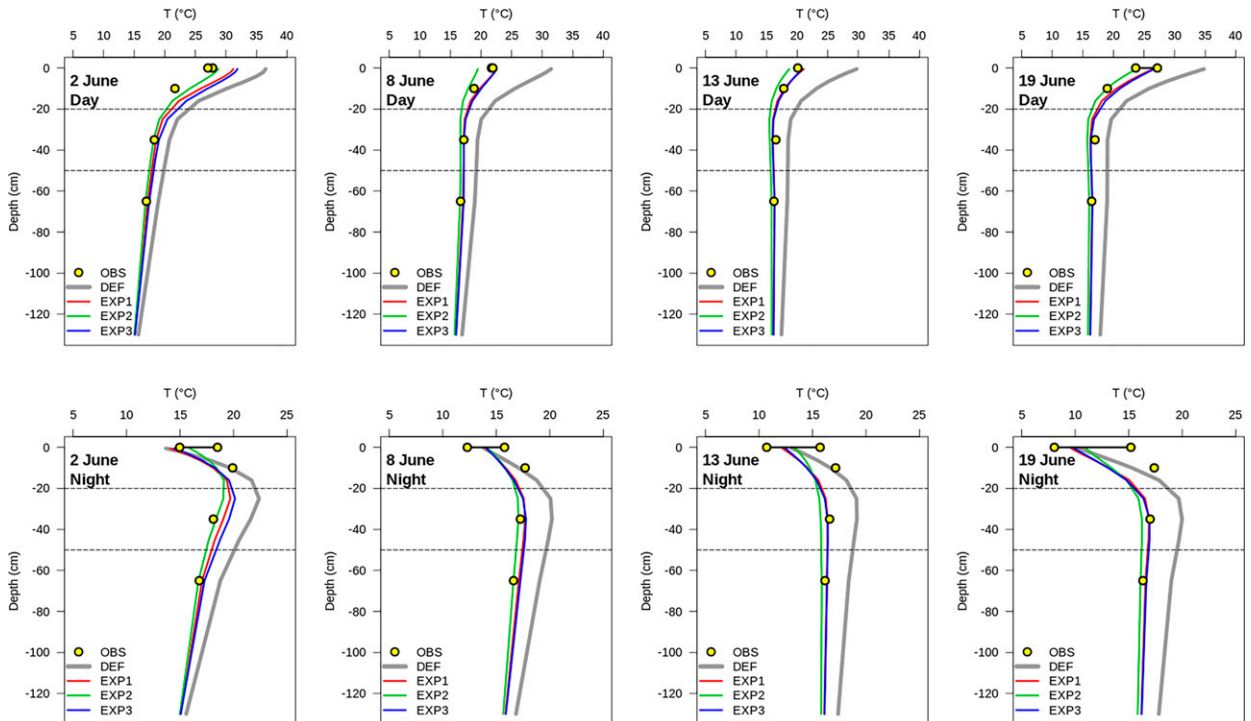


FIG. 9. Comparison of soil temperature profiles simulated by ISBA-DF according to the different configurations and in situ measurements for four selected dates during the field experiment at (top) night between 0100 and 0400 UTC and (bottom) day between 1300 and 1600 UTC.

layer for EXP1 and EXP2, probably because the high roughness of these two experiments maintains some convection that even if weak contribute to cooling the soil. In the deeper layers, both measured and simulated soil temperatures evolve little relative to those during the day. The results of EXP1 and EXP2 are in line with the observations. Nevertheless, a temperature profile that is more homogenized vertically over the soil column for EXP2 than for EXP1 is noted. Because the soil is a little wetter in EXP2, the thermal conductivity is slightly higher, which could explain this profile favored by more rapid thermal exchanges.

In summary, the comparison with the observations of the simulated soil temperatures and water contents with ISBA-DF according to the three experiments DEF, EXP1 and EXP2 indicates that the configuration EXP1 based on a defined aerodynamic roughness length at the garden scale (option Z0M-GARDEN = 0.32 m) gives the best scores. This finding confirms the hypothesis that the turbulent fluxes over the lawn are influenced by the urban elements in the immediate vicinity. Nonetheless, the soil texture option TXT-HWSD highlights important biases in the simulation of soil water status. It is expected that soil moisture and temperature simulation are sensitive to the prescription of soil properties, especially the soil texture parameters involved in pedotransfer functions used by ISBA-DF for the calculation of 1) the hydrological properties that control the capability of soil to retain or drain water and 2) the thermal properties that govern the heat conduction in the soil column. In the following

subsection, the potential contribution of a better prescription of the soil texture in the ISBA-DF soil column is considered.

c. Refinement of soil texture and properties

In urban areas, the subsurface soils (near the surface) are very heterogenous because they are heavily reworked during the civil works carried out for construction and maintenance of urban infrastructures. On the experimental site of Grand Clos, a characterization of the garden's soil texture has been performed by the Water and Environment Laboratory [l'Institut Français des Sciences et Technologies des Transports, de l'Aménagement et des Réseaux (IFSTTAR)] thanks to samples taken during the installation of the instrumentation. Measurements indicated a significant variability in soil texture with depth, with sand fractions of 60% at 10-cm depth, 50% at 35-cm depth, and 30% at 65-cm depth and clay fractions of 23% at 10-cm depth, 14% at 35-cm depth, and 30% at 65-cm depth. The current parameterization of ISBA-DF assumes a homogeneous texture of the soil column, which can be a strong limitation in representing the vertical heterogeneity of soil characteristics and potential impacts on water and heat transfer. Here, a modification has been implemented and tested in ISBA-DF in order to specify the vertical inhomogeneity of soil texture. The soil has been segregated into three layers (0–20, 20–50, and 50–180 cm) to which are attributed the measured values of sand and clay fractions. This new soil texture option is called TXT-INSITU. As for TXT-HWSD, the soil textures of the three layers are presented in Fig. 5

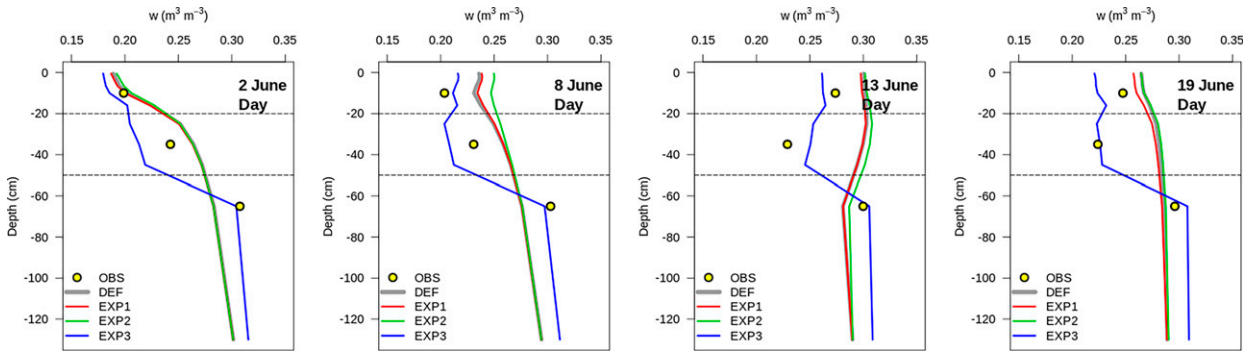


FIG. 10. Comparison of soil water content profiles simulated by ISBA-DF according to the different configurations and in situ measurements for four selected dates during the field experiment during the day between 1300 and 1600 UTC.

according to the standard soil taxonomy. It is here combined with the surface roughness option Z0M-GARDEN (chosen as it is the best performing) for conducting a new experience with ISBA-DF referred to as EXP3. The soil texture characteristics, as well as the soil thermal and hydrological properties derived from sand and clay fractions, are compiled in Table 1.

The prescription of field surveyed soil textures in ISBA-DF has a clear influence on soil moisture dynamics, which can be analyzed by comparing EXP1 and EXP3 experiments. The modification of sand and clay fractions impact the evolution of soil water contents at the three studied depths, but more significantly at 10- and 35-cm depths (Fig. 6 and Table 2). For these depths, the soil layers are characterized by more sandy soils in ISBA (Fig. 5), resulting mainly in higher hydraulic conductivities and lower matrix potentials at saturation, and a smaller available water capacity for the top layer (0.102 vs 0.155 m³ m⁻³ when compared with EXP1). The dynamics for soil moisture is consequently different, especially in the top layer, which is the most sensitive to water addition and turbulent fluxes and contains the root zone: the 37% lower matrix potential favors the loss of water by transpiration when meteorological conditions are conducive to the production of latent heat flux (as shown on Fig. 7 until 11 June) and higher hydraulic conductivities increase the speed of water transfers, both processes resulting in a more efficient soil drying in better agreement with observations. However, refined and more realistic the in situ soil texture might be, it should be noted that it does not take into account any organic matter that may have been present in the soil, especially that from the top layer of soil coming from the life cycle of the lawn or from amendment by the inhabitants of the garden. Not accounting for organic matter in the root zone of EXP3 has potentially underestimated the soil matrix potential to extract water as well as the speed of vertical water exchanges but this does not seem to impact simulation results during the period studied.

The evolution of water contents throughout the soil column is shown by following the water content profiles of four days chosen to highlight the behavior of the soil to different rainfall regimes (Fig. 10). Whatever the time/day, the soil water content at 65 cm with the in situ soil texture (EXP3)

systematically shows an improved agreement with observations although the refined texture is not very different from the HSWD texture (EXP1), which suggests that it is a consequence of a better simulation of water contents in the layers above. The inflections of the vertical profiles (Fig. 10) are well represented by the model under EXP3, with the middle layer between the root zone and the deep soil drying out in the course of the period simulated, while the deep layer reacts very little to surface fluctuations. In the root zone, the EXP3 shows the most realistic water content on 8 and 13 June, the least dry periods of the simulation.

The effect of texture is very small on the soil temperatures simulated by ISBA-DF (Fig. 8 and Table 2), which appear to be more driven by soil moisture status than by texture related changes in thermal characteristics. The main differences are observed in the first two soil layers (for the comparisons at 10- and 35-cm depths) for which the change in texture resulted in a slight increase in thermal conductivity (see Table 1). Temperatures are slightly warmer during the day, which further accentuates the positive biases already obtained for EXP1.

6. Conclusions

The soil-vegetation-atmosphere transfer ISBA-DF model was applied for a lawn located in a residential neighborhood, in order to evaluate the model's ability to simulate the evolution of the soil water and thermal status in an urban environment. The influence of local-scale roughness and soil characterization on the thermoradiative and hydrological behaviors of a garden lawn in a residential neighborhood was studied using observation-based and modeling approaches. When coupled with the urban canopy model TEB to model mixed urban environments (i.e., with the presence of vegetation), ISBA-DF usually follows a default configuration for the description of natural soil and vegetation characteristics. Especially, the surface roughness used for the calculation of turbulent fluxes (based on the MOST and big-leaf approach) is defined according to the type of vegetation, independently of any consideration of the immediate environment properties. The soil is described by a homogeneous texture of sand, clay, and silt throughout the column.

For the case study presented here, this configuration resulted in a systematic overestimation of soil temperatures, which is very clear at the surface but also remains throughout the soil column. The water contents simulated by ISBA-DF also exhibited substantial biases. It was shown that the key parameter in the improvement of soil temperature simulation, and especially of near-surface temperature, was the aerodynamic roughness length, which drives the surface energy exchanges (i.e., the turbulent fluxes Q_E and Q_H). Classically, ISBA-DF applies an aerodynamic roughness length linked to the height of the rough element (here the blade of grass). In our study case, an analysis of the roughness characteristics of the experimental site showed that the wind over the lawn surface could be considerably affected by the presence of nearby obstacles (garages, hedges, storerooms). This suggests that the horizontal homogeneity assumption of the MOST for the plant canopy is no longer valid within the urban canopy layer, so that the aerodynamic roughness length must be adapted to the complex environment. A value of 0.32 m was estimated, that is an intermediate value between the roughness of the grass blade of 0.004 m and the roughness of the whole urban canopy layer of 1.5 m. This configuration tested with ISBA-DF considerably improved the simulation of soil temperatures by amplifying heat transfers relative to the default configuration. According to this finding, the heat and water vapor transfers that took place between the lawn and the atmosphere seemed to be initiated by larger-scale turbulent motions generated by the local complex environment. They should be more properly modeled by adjusting the roughness parameter prescribed in ISBA-DF according to the surrounding obstacles. As shown in the present study, a simple morphometric approach can then be used to evaluate and prescribe a suitable aerodynamic roughness length. Although this study does not aim at a comprehensive revision of the MOST, it confirms its limitations inherent to heterogeneous environments, for the case of urban vegetation modeling. Some land surface models now included roughness sublayer parameterizations to correct the MOST theoretical vertical profiles of wind and temperature within and above tree canopies (Bonan et al. 2018; Lee et al. 2020), which could potentially be extended to urban canopies (Theeuwes et al. 2019). Nonetheless, the problem is twofold here, by considering the more local question of the plant canopy within the urban canopy layer. A very-high-resolution modeling approach (such as with computational fluid dynamics models) could help in a more accurate calculation of the exchange coefficients for the road and the vegetation, but a generalization of the formulation for mesoscale modeling is far from trivial.

Another important conclusion of this study was to highlight that a better prescription of the soil texture profile provided more realistic soil hydrological properties. By doing this, the vertical water transfers and evolution of water contents were better simulated. To date, few soil databases provide information on several depth levels. One example is the global Soil-Grids250m (Hengl et al. 2017) database, which provides sand, clay, and loam fractions at 0, 5, 15, 30, 60, 100, and 200 cm. However, there is still a great uncertainty about the qualification of urban soils, which have the particularity of being

reworked and very heterogeneous. Finally, it can be noted that in addition to the modification of soil texture, additional sensitivity tests were carried out. Prescribed values for lawn leaf area index and grass root profile were tested within realistic ranges, but the model response to these changes showed little variability in both soil temperatures and water content.

Acknowledgments. This work was supported by the French research projects VegDUD funded by the Agence Nationale de la Recherche (ref ANR-09-VILL-0007) and Rosenhy funded by the EC2CO program from the Institut National des Sciences de l'Univers (2011–13). The authors thank the owners of the garden, Mr. and Mrs. Blanchetière, for permission to install the instrumentation systems during the FluxSAP campaign. They also thank Sandrine Marc for authorizing the publication of her photograph of the Grand-Clos neighborhood (Fig. 1).

Data availability statement. The ISBA code is included in the official version of SURFEX v8.1 (<http://www.umr-cnrm.fr/surfex/>). The experimental data and model outputs used in this study are available in open access on Zenodo (<https://doi.org/10.5281/zenodo.5482804>).

REFERENCES

- Bagga, I., 2012: Mesure et analyse des flux thermo-hydriques en zone urbaine hétérogène. Ph.D. thesis, Ecole Centrale de Nantes, 212 pp.
- Banerjee, T., F. D. Roo, and M. Mauder, 2017: Explaining the convective effect in canopy turbulence by means of large-eddy simulation. *Hydrol. Earth Syst. Sci.*, **21**, 2987–3000, <https://doi.org/10.5194/hess-21-2987-2017>.
- Berry, R., S. Livesley, and L. Aye, 2013: Tree canopy shade impacts on solar irradiance received by building walls and their surface temperature. *Build. Environ.*, **69**, 91–100, <https://doi.org/10.1016/j.buildenv.2013.07.009>.
- Bonan, G., E. Patton, I. Harman, K. Oleson, J. Finnigan, Y. Lu, and E. Burakowski, 2018: Modeling canopy-induced turbulence in the earth system: A unified parameterization of turbulent exchange within plant canopies and the roughness sublayer (CLM-ml v0). *Geosci. Model Dev.*, **11**, 1467–1496, <https://doi.org/10.5194/gmd-11-1467-2018>.
- Boone, A., J. Calvet, and J. Noilhan, 1999: Inclusion of a third layer in a land surface scheme using the force restore. *J. Appl. Meteor.*, **38**, 1611–1630, [https://doi.org/10.1175/1520-0450\(1999\)038<1611:IOATSL>2.0.CO;2](https://doi.org/10.1175/1520-0450(1999)038<1611:IOATSL>2.0.CO;2).
- , V. Masson, T. Meyers, and J. Noilhan, 2000: The influence of the inclusion of soil freezing on simulations by a soil-vegetation-atmosphere transfer scheme. *J. Appl. Meteor.*, **39**, 1544–1569, [https://doi.org/10.1175/1520-0450\(2000\)039<1544:TIOTIO>2.0.CO;2](https://doi.org/10.1175/1520-0450(2000)039<1544:TIOTIO>2.0.CO;2).
- Christen, A., and R. Vogt, 2004: Energy and radiation balance of a central European city. *Int. J. Climatol.*, **24**, 1395–1421, <https://doi.org/10.1002/joc.1074>.
- Daniel, M., A. Lemonsu, and V. Vigié, 2018: Role of watering practices in large-scale urban planning strategies to face the heat-wave risk in future climate. *Urban Climate*, **23**, 287–308, <https://doi.org/10.1016/j.uclim.2016.11.001>.
- Decharme, B., A. Boone, C. Delire, and J. Noilhan, 2011: Local evaluation of the Interaction between Soil Biosphere

- Atmosphere soil multilayer diffusion scheme using four pedo-transfer functions. *J. Geophys. Res.*, **116**, D20126, <https://doi.org/10.1029/2011JD016002>.
- de Munck, C., A. Lemonsu, R. Bouzoudja, V. Masson, and R. Claverie, 2013: The GREENROOF module (v7.3) for modelling green roof hydrological and energetic performances within TEB. *Geosci. Model Dev.*, **6**, 1941–1960, <https://doi.org/10.5194/gmd-6-1941-2013>.
- , —, V. Masson, J. Le Bras, and M. Bonhomme, 2018: Evaluating the impacts of greening scenarios on thermal comfort and energy and water consumptions for adapting Paris city to climate change. *Urban Climate*, **23**, 260–286, <https://doi.org/10.1016/j.uclim.2017.01.003>.
- Erbs, D., S. Klein, and J. Duffie, 1982: Estimation of the diffuse radiation fraction for hourly, daily and monthly-average global radiation. *Sol. Energy*, **28**, 293–302, [https://doi.org/10.1016/0038-092X\(82\)90302-4](https://doi.org/10.1016/0038-092X(82)90302-4).
- FAO/IIASA/ISRIC/ISSCAS/JRC, 2012: Harmonized World Soil Database (version 1.2). FAO and IIASA, accessed 7 September 2021, <https://www.fao.org/soils-portal/data-hub/soil-maps-and-databases/harmonized-world-soil-database-v12/en/>.
- Green, A., G. Bohrer, and R. Petrone, 2021: Microclimatic effects of a forest-to-peatland transition on aerodynamic resistance to water vapour transfer in the sub-humid boreal plains. *Bound.-Layer Meteor.*, **178**, 301–322, <https://doi.org/10.1007/s10546-020-00572-3>.
- Hengl, T., and Coauthors, 2017: SoilGrids250m: Global gridded soil information based on Machine Learning. *PLOS ONE*, **2**, e0169748, <https://doi.org/10.1371/journal.pone.0169748>.
- Kent, C. W., K. Lee, H. C. Ward, J.-W. Hong, J. Hong, D. Gatey, and S. Grimmond, 2018: Aerodynamic roughness variation with vegetation: Analysis in a suburban neighbourhood and a city park. *Urban Ecosyst.*, **21**, 227–243, <https://doi.org/10.1007/s11252-017-0710-1>.
- Krayenhoff, E. S., A. Christen, A. Martilli, and T. R. Oke, 2014: A multi-layer radiation model for urban neighbourhoods with trees. *Bound.-Layer Meteor.*, **151**, 139–178, <https://doi.org/10.1007/s10546-013-9883-1>.
- , J.-L. Santiago, A. Martilli, A. Christen, and T. Oke, 2015: Parametrization of drag and turbulence for urban neighbourhoods with trees. *Bound.-Layer Meteor.*, **156**, 157–189, <https://doi.org/10.1007/s10546-015-0028-6>.
- , and Coauthors, 2020: A multi-layer urban canopy meteorological model with trees (BEP-Tree): Street tree impacts on pedestrian-level climate. *Urban Climate*, **32**, 100590, <https://doi.org/10.1016/j.uclim.2020.100590>.
- , and Coauthors, 2021: Cooling hot cities: A systematic and critical review of the numerical modelling literature. *Environ. Res. Lett.*, **16**, 053007, <https://doi.org/10.1088/1748-9326/abdcf1>.
- Lee, J., J. Hong, Y. Noh, and P. Jiménez, 2020: Implementation of a roughness sublayer parameterization in the Weather Research and Forecasting model (WRF version 3.7.1) and its evaluation for regional climate simulations. *Geosci. Model Dev.*, **13**, 521–536, <https://doi.org/10.5194/gmd-13-521-2020>.
- Lee, S.-H., 2011: Further development of the vegetated urban canopy model including a grass covered surface parameterization and photosynthesis effects. *Bound.-Layer Meteor.*, **140**, 315–342, <https://doi.org/10.1007/s10546-011-9603-7>.
- , and S.-U. Park, 2008: A vegetated urban canopy model for meteorological and environmental modelling. *Bound.-Layer Meteor.*, **126**, 73–102, <https://doi.org/10.1007/s10546-007-9221-6>.
- Lemonsu, A., V. Masson, L. Shashua-Bar, E. Erell, and D. Pearlmutter, 2012: Inclusion of vegetation in the Town Energy Balance model for modelling urban green areas. *Geosci. Model Dev.*, **5**, 1377–1393, <https://doi.org/10.5194/gmd-5-1377-2012>.
- Litvak, E., N. S. Bijoer, and D. E. Pataki, 2014: Adding trees to irrigated turfgrass lawns may be a water-saving measure in semi-arid environments. *Ecohydrology*, **7**, 1314–1330, <https://doi.org/10.1002/eco.1458>.
- Monin, A., and A. Obukhov, 1954: Basic laws of turbulent mixing in the atmosphere near the ground. *Tr. Geofiz. Inst., Akad. Nauk SSSR*, **24**, 163–187.
- Noilhan, J., and S. Planton, 1989: A simple parameterization of land surface processes for meteorological models. *Mon. Wea. Rev.*, **117**, 536–549, [https://doi.org/10.1175/1520-0493\(1989\)117<0536:ASPOLS>2.0.CO;2](https://doi.org/10.1175/1520-0493(1989)117<0536:ASPOLS>2.0.CO;2).
- Oke, T. R., 1982: Advectionally-assisted evapotranspiration from irrigated urban vegetation. *Bound.-Layer Meteor.*, **17**, 167–173, <https://doi.org/10.1007/BF00117976>.
- , G. Mills, A. Christen, and J. A. Voogt, 2017: *Urban Climates*. Cambridge University Press, 546 pp., <https://doi.org/10.1017/9781139016476>.
- Pataki, D. E., H. R. McCarthy, E. Litvak, and S. Pincetl, 2011: Transpiration of urban forests in the Los Angeles metropolitan area. *Ecol. Appl.*, **21**, 661–677, <https://doi.org/10.1890/09-1717.1>.
- Qin, Z., and A. Karnieli, 1999: Progress in the remote sensing of land surface temperature and ground emissivity using NOAA-AVHRR data. *Int. J. Remote Sens.*, **20**, 2367–2393, <https://doi.org/10.1080/014311699212074>.
- Redon, E., A. Lemonsu, V. Masson, B. Morille, and M. Musy, 2017: Implementation of street trees within the solar radiative exchange parameterization of TEB in SURFEXv8.0. *Geosci. Model Dev.*, **10**, 385–411, <https://doi.org/10.5194/gmd-10-385-2017>.
- , —, and —, 2020: An urban trees parameterization for modeling microclimatic variables and thermal comfort conditions at street level with the Town Energy Balance model (TEB-SURFEX v8.0). *Geosci. Model Dev.*, **13**, 385–399, <https://doi.org/10.5194/gmd-13-385-2020>.
- Rodriguez, F., and Coauthors, 2015: FluxSAP—A collaborative experimental campaign on water and energy fluxes in urban areas and the relation with the vegetation: The case of a Nantes district. *Ninth Int. Conf. on Urban Climate*, Toulouse, France, Météo-France, 7.4, <http://www.meteo.fr/ctic9/presentations/NOMTM/NOMTM7-4.pdf>.
- Ruban, V., F. Rodriguez, J.-M. Rosant, F. Larrarte, C. Joannis, P. Mestayer, and H. Andrieu, 2007: Hydrologic and energetic experimental survey of a small urban watershed. *Sixth Int. Conf. on Sustainable Techniques and Strategies in Urban Water Management*, Lyon, France, GRAIE, 6.1., <https://hal.archives-ouvertes.fr/hal-03238905/document>.
- Ryu, Y., E. Bou-Zeid, Z. Wang, and J. Smith, 2016: Realistic representation of trees in an urban canopy model. *Bound.-Layer Meteor.*, **159**, 193–220, <https://doi.org/10.1007/s10546-015-0120-y>.
- Santamouris, M., 2013: Using cool pavements as a mitigation strategy to fight urban heat island—A review of the actual developments. *Renewable Sustainable Energy Rev.*, **26**, 224–240, <https://doi.org/10.1016/j.rser.2013.05.047>.
- Shashua-Bar, L., D. Pearlmutter, and E. Erell, 2009: The cooling efficiency of urban landscape strategies in a hot dry climate. *Landscape Urban Plann.*, **92**, 179–186, <https://doi.org/10.1016/j.landurbplan.2009.04.005>.
- Snyder, R., C. Pedras, A. Montazar, J. Henry, and D. Ackley, 2015: Advances in ET-based landscape irrigation management. *Agric. Water Manage.*, **147**, 187–197, <https://doi.org/10.1016/j.agwat.2014.07.024>.

- Souch, C., 1993: The effect of trees on summertime below canopy urban climates: A case study, Bloomington, Indiana. *J. Arboric.*, **19**, 303–312.
- Templeton, N. P., E. R. Vivoni, Z.-H. Wang, and A. P. Schreiner-McGraw, 2018: Quantifying water and energy fluxes over different urban land covers in Phoenix, Arizona. *J. Geophys. Res.*, **123**, 2111–2128, <https://doi.org/10.1002/2017JD027845>.
- Theeuwes, N. E., R. J. Ronda, I. N. Harman, A. Christen, and C. S. B. Grimmond, 2019: Parametrizing horizontally-averaged wind and temperature profiles in the urban roughness sublayer. *Bound.-Layer Meteor.*, **173**, 321–348, <https://doi.org/10.1007/s10546-019-00472-1>.
- Wang, Z.-H., E. Bou-Zeid, and J. A. Smith, 2013: A coupled energy transport and hydrological model for urban canopies evaluated using a wireless sensor network. *Quart. J. Roy. Meteor. Soc.*, **139**, 1643–1657, <https://doi.org/10.1002/qj.2032>.
- Zhao, Q., J. Yang, Z.-H. Wang, and E. A. Wentz, 2018: Assessing the cooling benefits of tree shade by an outdoor urban physical scale model at Tempe, AZ. *Urban Sci.*, **2**, 4, <https://doi.org/10.3390/urbansci2010004>.